Multiplex imaging of quantal glutamate release and presynaptic Ca^{2+} at multiple synapses *in situ*

Thomas P. Jensen[1], Kaiyu Zheng[1], Nicholas Cole[1], Jonathan S. Marvin[2], Loren L. Looger[2], Dmitri A. Rusakov[1]

[1]UCL Institute of Neurology, University College London, Queen Square, London WC1N 3BG, UK

[2]Janelia Research Campus, Howard Hughes Medical Institute, Ashburn, Virginia, USA

Correspondence: Dmitri Rusakov (d.rusakov@ucl.ac.uk) or Thomas Jensen (t.jensen@ucl.ac.uk)

Information processing by brain circuits depends on Ca^{2+}-dependent, stochastic release of the excitatory neurotransmitter glutamate. Recently developed optical sensors have enabled detection of evoked and spontaneous release at common glutamatergic synapses. However, monitoring synaptic release probability, its use-dependent changes, and its underpinning presynaptic machinery *in situ* requires concurrent, intensity-independent readout of presynaptic Ca^{2+} and glutamate release. Here, we find that the red-shifted Ca^{2+} indicator Cal-590 shows Ca^{2+}-sensitive fluorescence lifetime, and employ it in combination with the novel green glutamate sensor SF-iGluSnFR variant to document quantal release of glutamate together with presynaptic Ca^{2+} concentration, in multiple synapses in an identified neural circuit. At the level of individual presynaptic boutons, we use multi-exposure and stochastic reconstruction procedures to reveal nanoscopic co-localisation of presynaptic Ca^{2+} entry and glutamate release, a fundamental unknown in modern neurobiology. This approach opens a new horizon in the quest to understand release machinery of central synapses.

Stochastic, Ca^{2+}-dependent release of the excitatory neurotransmitter glutamate by individual synapses is what underpins information handling and storage by neural networks. However, in many central circuits glutamate release occurs with a low probability and a high degree of heterogeneity among synapses [1, 2] . Therefore, methods to probe presynaptic function in an intact brain aim to reliably detect presynaptic action potentials, record the presynaptic Ca^{2+} dynamics, and register release of individual glutamate quanta with high temporal resolution and broad dynamic range. The optical quantal analysis method went some way toward this goal, by providing quantification of release probability at individual synapses in brain slices [3, 4]. In parallel, advances in the imaging techniques suited to monitor membrane retrieval at presynaptic terminals have enabled detection of synaptic vesicle exocytosis in cultured neurons [5]. Recently developed optical glutamate sensors [6, 7] have drastically expanded the sensitivity and the dynamic range of glutamate discharge detection in organised brain tissue [8]. However, such methods on their own cannot relate neurotransmitter release to presynaptic Ca^{2+} dynamics, which

is the key to understanding presynaptic release machinery, as demonstrated in elegant studies of giant synapses permitting direct electrophysiological probing [9-11].

Furthermore, conventional methods of optical detection based on fluorescence intensity measures face multiple challenges when applied in turbid media such as organised brain tissue. Registered emission intensity can be strongly affected by focal drift, photobleaching, or any experimental concomitants (such as cell swelling or temperature fluctuations) impacting on light scattering. To overcome such difficulties in Ca^{2+} imaging, we have recently developed a technique to employ Ca^{2+}-sensitive fluorescence lifetime of the Ca^{2+} indicator OGB-1 [8, 12, 13]. The FLIM readout provides nanomolar-range Ca^{2+} sensitivity and is insensitive to light scattering, dye concentration, focus drift or photobleaching. However, OGB-1 emission is chromatically inseparable from that of existing glutamate sensors, thus prohibiting simultaneous imaging of glutamate release [8]. To deal with this challenge, we have systematically explored time-resolved fluorescence properties of Ca^{2+} indicators and discovered that the fluorescence lifetime of red-shifted Cal-590, an indicator that has been successfully used in deep-brain imaging [14], is also sensitive to low nanomolar Ca^{2+}.

In parallel, we have developed a glutamate sensor variant SF-iGluSnFR.A184S whose kinetic properties permit reliable registration of individual quanta of released neurotransmitter at multiple glutamate release sites. The ability to discern quantal release is important for enabling a fluorescence intensity-insensitive monitoring of release probability, by relying on counting individual released quanta rather than on the signal amplitude readout. We took advantage of these findings and used organotypic brain slice preparations to demonstrate, in multiplex imaging mode, chromatic separation of concurrent signals reporting glutamate release and presynaptic Ca^{2+}, at multiple individual synapses hosted by traced cell axons. The method thus enables the monitoring of synaptic release probability, its use-dependent changes, and the underpinning Ca^{2+} machinery in an identified brain circuit *in situ*.

Intriguingly, the fact that Ca^{2+} -sensitive FLIM readout does not scale with dye concentration (or dye sampling volume) and that iGluSnFR.A184S is confined to the membrane surface has provided a unique opportunity to localise Ca^{2+} and glutamate hotspots in individual presynaptic boutons on the sub-diffraction scale. Thus, we combined multiplex imaging with repeated exposure and stochastic localisation routines to evaluate nanoscopic co-localisation of presynaptic Ca^{2+} entry and glutamate release sites, a fundamental neurobiological issue [15, 16].

RESULTS

FLIM readout of red-shifted Cal-590 reports low presynaptic Ca^{2+}

In search of suitable red-shifted Ca^{2+} indicators we tested and excluded the classical rhodamine-based dyes: they appear highly lipophilic, a property undesirable for imaging in axons where free cytosolic diffusion is required to obtain sufficient indicator level away from the soma. Because the fluorescein-based, red shifted Cal-590 was previously found to provide reliable Ca^{2+} monitoring for deep brain imaging *in vivo* [14], we set about testing the Ca^{2+} sensitivity of its fluorescence lifetime, particularly for two-photon excitation at λ_x^{2p} ~910 nm, alongside the green glutamate sensor iGluSnFR [6, 7]. We discovered a clear dependence between the Cal-590 fluorescence lifetime and [Ca^{2+}] using a series of Ca^{2+}-clamped solutions, as described

previously [17, 18] (Fig. 1a). This dependence was most pronounced around λ_x^{2p} ~ 910 nm (Supplementary Fig. 1a) and appeared largely insensitive to temperature (and associated viscosity changes) between 20-37ºC (Supplementary Fig. 1b). Several other tested Ca^{2+} indicators, including red-shifted Asante Calcium Red and Calcium Ruby-nano, showed no usable [Ca^{2+}] sensitivity in their fluorescence lifetime (Supplementary Fig. 1c).

Aiming to calibrate Cal-590 lifetime to [Ca^{2+}], we used the protocol established previously for OGB-1 [17, 18]. It employs the Normalised Total Count (NTC) method in which photon counts are integrated across the Ca^{2+} sensitive components of the lifetime decay curve (rather than fitted by multi-exponentials). This method substantially lowers the minimum requirement for the photon counts, which in turn shortens minimal acquisition time and improves spatiotemporal resolution of Ca^{2+} imaging [17, 18]. Quantitative calibration of Cal-590 showed the greatest sensitivity in the 0-200 nM range (Fig. 1b).

To verify that this approach could be applied in axons traced in organised brain tissue, we turned to organotypic hippocampal brain slices. Because Cal-590 could not be reliably used for axon tracing (due to its weak emission at low baseline [Ca^{2+}]) we employed the bright fluorescence of iGluSnFR, under conditions of sparse cell labelling. We biolistically transfected iGluSnFR in slice preparations (Methods), patch-loaded iGluSnFR-expressing CA3 pyramidal cells with Cal-590 (300 µM), and traced their axonal boutons for at least 150-200 microns from the cell soma, towards area CA1 (Fig. 1c). We imaged the axonal bouton of interest using a spiral ('tornado') scanning mode (Fig. 1c, bottom), which we showed to enable rapid (1-2 ms) coverage of the bouton area during single sweeps [8]. Thus, to assess the dynamic range of Cal-590 FLIM readout *in situ*, we recorded both intensity and lifetime decay of the axonal signal in low Ca^{2+} resting conditions (for ~400 ms), followed by a 50 ms, 100 Hz burst of spikes evoked at the soma (Fig. 1d), which should reliably saturate the indicator [19, 20]. Comparing the respective Cal-590 fluorescence decay curves confirmed a wide dynamic range of [Ca^{2+}] sensitivity (Fig. 1e), consistent with the calibration data *in vitro* (Fig. 1a-b).

Glutamate sensor SF-iGluSnFR.A184S enables multi-synapse monitoring of quantal release

We next asked whether the kinetic features of available glutamate sensors (iGluSnFR family) were suited for simultaneous imaging of multiple axonal boutons. This consideration was important because the laser beam has to dwell for 1-2 ms at each bouton to achieve signal-to-noise ratio comparable with that obtained under tornado-scanning of individual boutons [8]. Thus, reliable imaging of fluorescent signals concurrently at 4-5 locations requires the signals to last (preferably near its peak) for at least 10-15 ms. Fortuitously, this requirement is normally met by high-affinity Ca^{2+} indicators including Cal-590 [14].

We thus found that the kinetics of the recently developed glutamate sensor variant SF-iGluSnFR.A184S [7] was suited to reliably report quantal release of glutamate from at least four axonal boutons simultaneously (Fig. 1f-g). The indicator provided stable recordings, with no detectable photobleaching, over multiple trials, thus enabling direct readout of release probability at multiple synapses from the same circuitry (Fig. 1h).

Simultaneous monitoring of quantal glutamate release and presynaptic Ca^{2+} dynamics

Equipped with Cal-590 calibration and optimal iGluSnFR kinetics, we set out to simultaneously monitor glutamate release and presynaptic Ca^{2+} at individually traced axonal boutons of CA3 pyramidal cells, as described above (Fig. 1c, Fig. 2a). To document basal presynaptic function and its short-term plasticity, we recorded fluorescent responses to a short burst of four evoked action potentials at 20 Hz, a pattern of activation which falls well within the range documented for CA3-CA1 connections *in vivo* [21].

For method illustration purposes, fluorometric responses for glutamate and Ca^{2+} were analysed in two boutons supplied by the same axon. The signals were fully chromatically separated (Fig. 2b) and readily reported individual quantal releases of glutamate in single-sweep recordings, with high resolution and excellent signal-to-noise ratio (Fig. 2c). The average glutamate release kinetics indicated a much higher release efficacy in bouton 1 compared to bouton 2, which corresponded to the relative short-term depression and facilitation, respectively, shown by the two synapses (Fig. 2d). Reassuringly, the quantal size (iGluSnFR signal corresponding to the release of one glutamate vesicle) remained stable throughout the trials (Supplementary Fig. 2a).

In the Cal-590 channel, the emission intensity reporting the average presynaptic Ca^{2+} dynamics (recorded simultaneously with glutamate release detection) was indistinguishable between the boutons (Fig. 2e) whereas FLIM readout suggested somewhat lower Ca^{2+} levels (basal and evoked transient) in bouton 2 (Fig. 2f). A detailed investigation of these relationships is intriguing but falls beyond the scope of the present methodological study: the data presented here demonstrate the possibilities of functional synaptic monitoring provided by the method. In this context, one important consideration is that any Ca^{2+} indicator, by buffering intracellular Ca^{2+}, could interfere with endogenous Ca^{2+} dynamics and thus neurotransmitter release properties. However, when we compared axonal boutons between iGluSnFR-expressing CA3 pyramidal cells loaded, and not loaded, with Cal-590, the average detected release probabilities were indistinguishable (Supplementary Fig. 2b). This observation suggests that Cal-590 loading did not affect synaptic properties and lends further support to the physiological relevance of the method (see Discussion for details).

Nanoscopic co-localisation of presynaptic glutamate release and Ca^{2+} entry

Action potentials arriving at the presynaptic bouton drive open local Ca^{2+} channels: the ensuing rapid Ca^{2+} entry triggers neurotransmitter release, in a probabilistic fashion. The effective distance between the (predominant) Ca^{2+} entry site and the release triggering site (SNARE protein complex) is considered a key factor in determining release probability hence synaptic efficacy [15, 16, 22]. What this typical distance is, whether it changes in a use-dependent manner, whether the loci of presynaptic Ca^{2+} entry and glutamate release 'migrate', and whether different modes of release (spontaneous as opposed to evoked) correspond to different loci remain highly debated issues.

To understand whether these issues could be approached by multiplex imaging in the current context, we looked at the nanoscopic features of the optical settings employed. Here, individual axonal boutons express a membrane-bound (green) glutamate sensor and a cytosolic (red) Ca^{2+} indicator (Fig. 3a). The inherent blur in the imaged bouton is due to the fact that excitation and emission follow the 'probability cloud' set by the system's point-spread function (PSF), which is determined in large part by the optical diffraction limit. In a well-tuned two-photon excitation

microscope, the PSF is expected to be in the range of 0.2-0.3 µm in the (focal, *x*-*y*) plane of view, and 0.8-1.2 µm in the *z* direction, although the latter is effectively larger due to focus fluctuations. Thus, a spiral (tornado) laser scan of an axonal bouton normally provides roughly uniform excitation, with optical resolution of 0.2-0.3 µm in the focal plane, while integrating the fluorometric signal in the *z* direction (Fig. 3b). In other words, the imaged bouton in the current settings reflects its *z*-axis projection onto the *x*-*y* (focal) plane. Can we improve resolution in the focal plane, to localise fluorescent events on the nanoscale?

Both glutamate vesicle release and Ca^{2+} entry generate very steep diffusion gradients, with their concentrations falling orders of magnitudes over tens of nanometers from the site of action [15, 16, 18, 22, 23]. Thus, the respective fluorescent signals must concentrate at highly localised, nanoscopic hotspots (Fig. 3c, left). The corresponding fluorometric readout is however blurred by the PSF as well as by inherent optical noise, such as shot noise and mechanical fluctuations (Fig. 3c, middle). The noise can be reduced using multiple image exposure whereas the PSF centroid (or its brightest part) could provide simple 'stochastic localisation' of the signal origin (assuming that its location remains unchanged) (Fig. 3c, right).

In an attempt to implement this approach, we first mapped (20-trial average) the iGluSnFR signal across the visible axonal bouton (Fig. 3d, top). However, this image represents an *x*-*y* projection of the fluorescence signals originating from the axonal surface (see above and Fig. 3b). Thus, the signal registered near the visible bouton edges will strongly overestimate its intensity in 3D, which can be illustrated by a projection of a sphere with an even distribution of surface points (Fig. 3d, bottom). The underlying geometry indicates that, for any selected point in the projected image the factor to correct such overestimation is $cos(\varphi)$ (spherical coordinate; Fig. 3e, top; Supplementary Fig. 3a-b). The latter could be readily estimated from the point position relative to the visible bouton boundary (Supplementary Fig. 3a-b). By implementing this correction factor we therefore obtained localisation of the expected glutamate release site(s) on the nanoscale (Fig. 3e, bottom; Supplementary Fig. 3c; see Discussion for the uncertainties involved).

In contrast, the average fluorometric intensity signal for Ca^{2+} (Fig. 3f) should scale with the volume of the indicator within the bouton (Fig. 3b). However, the corresponding FLIM readout does not depend on the indicator volume or signal intensity and therefore should provide unbiased, albeit noisy, event localisation in the *x*-*y* plane (*z* localisation remains uncertain). Again, reducing the noise through multiple exposures enables nanoscopic localisation of Ca^{2+} entry (Fig. 3g). Intriguingly, in this example the sites of expected Ca^{2+} entry and glutamate release appear to show nanoscopic colocalisation (Fig. 3e and g; however, see Discussion). Clearly, a separate dedicated study is required to investigate this further.

DISCUSSION

FLIM monitoring of low presynaptic Ca^{2+} with Cal-590

In this study we have established that the fluorescence lifetime of red-shifted Ca^{2+} indicator Cal-590 is sensitive to $[Ca^{2+}]$ in the 10-200 nM range, with an optimal two-photon excitation wavelength of ~910 nm. We have calibrated this dependence using the normalised photon counting protocol described earlier [12, 13] and thus been able to obtain direct readout of $[Ca^{2+}]$

dynamics in neuronal axons using whole-cell dialysis of CA3 pyramidal cells with Cal-590 in organotypic brain slice preparations. The knowledge about low basal [Ca^{2+}] and its changes in neuronal axons is fundamentally important for understanding the machinery of neurotransmitter release. This is because free [Ca^{2+}] level is a reflection of equilibrium between local Ca^{2+} entry, removal, and binding-unbinding with local Ca^{2+} buffers. Thus, changes in low [Ca^{2+}] not only report a shifted equilibrium, they directly alter the availability (and thus buffering capacity) of Ca^{2+}-free endogenous Ca^{2+} buffers [24-26]. As the bound-to-free ratio for presynaptic Ca^{2+} varies between 100-1000-fold [19, 22, 27], equilibrated basal Ca^{2+} must contribute strongly to the spatiotemporal integration of intracellular Ca^{2+} 'hotspots' hence the triggering of release [15, 16].

In addition to high [Ca^{2+}] sensitivity in the nanomolar range, at least in the case of OGB-1 or Cal-590, a critical technical advantage of the FLIM readout is that it does not depend on the dye amount or concentration, light scattering, focus fluctuations, and other concomitants of live imaging [12, 13]. The latter is particularly important for imaging in freely-moving animals. Having a relatively more complicated procedure to record and analyse FLIM recordings compared to standard fluorometric monitoring [12, 13] appears a small price to pay for such advantages.

Intracellular Ca^{2+} buffering by Cal-590

Because Ca^{2+} indicators are by definition Ca^{2+} buffers they could affect intracellular Ca^{2+} homeostasis. Our recent study has shown, however, that moderate increases in the intracellular concentration of OGB-1 has little influence on the cell-wide landscape of low basal Ca^{2+} in principal neurons [12]. This is because inside cells the steady-state, equilibrated [Ca^{2+}] level depends on the action of Ca^{2+} sources and sinks which in turn are controlled by active [Ca^{2+}] sensing mechanisms rather than by 'passive' Ca^{2+} buffers [25]. However, the effect of Ca^{2+} indicators on rapid presynaptic Ca^{2+} dynamics and release probability could be significant, as we demonstrated previously [19, 28]. Cal-590 has a relatively low affinity (K_d ~ 560 nM) compared to OGB-1 (K_d ~ 170-260 nM) [11, 29], and should therefore have an even lower Ca^{2+} buffering effect. Intriguingly, we found no significant effect of axon loading with Cal-590 on the average release probability. Whilst this speaks in favour of the method, the physiological implications of this observation, in terms of the presynaptic mechanisms involved, require a separate study. Reassuringly, it was earlier reported that bolus-loading application of Cal-590 was fully compatible with intense network spiking activity in the visual cortex *in vivo* [14]. Furthermore, Ca^{2+} indicators with higher affinity, such as OGB-1 or some genetically-encoded Ca^{2+} indicators, have been widely used to register and manipulate neural network activity in freely-moving animals, without apparent behavioural implications [30, 31]. In any case, a more systematic comparison of release probabilities among axons loaded with Cal-590 at different concentrations, within the same synaptic circuitry, are required to quantitatively assess potential subtle effects of the dye.

Multiplex monitoring of presynaptic function

Enabling simultaneous readout of presynaptic Ca^{2+} dynamics and quantal glutamate release at small central synapses *in situ* is important at least for two reasons. Firstly, it enables a monitoring regime of release probability that is insensitive (or only weakly sensitive) to the fluorescence emission intensity registered in organised brain tissue. Thus, the common concomitants of live imaging *in situ* or *in vivo*, such as focus drift, photobleaching, or physiological changes in tissue light scattering or absorption should have only a limited effect on

the release probability readout with the present multiplex approach. Furthermore, axonal Ca^{2+} monitoring *in vivo* is essential for presynaptic spike detection: the efficiency of (bolus-applied) Cal-590 in registering action potentials in deep brain imaging settings has recently been demonstrated [14]. Thus, comparing the occurrence of spikes (Ca^{2+} channel) with the statistics of stochastic glutamate release events (iGluSnFR channel) at individual axonal boutons should provide a quantitative gauge of synaptic transmission fidelity, and its use-dependent changes, in such experiments.

Secondly, the method should provide key insights into the mechanistic relationship between Ca^{2+} entry and release probability, and how this relationship changes during use-dependent synaptic plasticity. To address such fundamental questions, classical studies in giant (Calyx) synapse preparations combined presynaptic Ca^{2+} imaging with patch-clamp recordings in pre- and/or postsynaptic structures, which were large enough to allow access [9, 10, 32]. Whilst such studies have been pivotal for understanding the basics of Ca^{2+}-dependent release machinery, to what degree their conclusions could be extrapolated to diverse neural circuits, in different brain regions, remains poorly understood. In this context, it is particularly important to have reliable readout of low basal Ca^{2+}, which directly affects the amount of available endogenous Ca^{2+} buffers and release probability (see above) [10].

Importantly, the kinetics of the glutamate sensor variant SF-iGluSnFR.A184S (as well as the kinetics of Cal-590) used in this study were well suited to monitor release probability at multiple synapses supplied by the same axon. Thus, the method enables real-time readout of heterogeneous presynaptic identities, their possible collective or cooperative features, and their plasticity within an identified synaptic circuit.

On a technical note, with the present method, we used the basal iGluSnFR fluorescence signal, under sparse expression of the indicator, to trace individual cell axons. Clearly, this axonal tracing approach could be adapted to the use of other appropriate dyes and genetically encoded indicators (such as a red-shifted version of iGluSnFR [33] or sensors for other neurotransmitters), or other sparse transfection methods, to enable simultaneous multi-target *in vivo* functional imaging.

Nanoscopic co-localisation of presynaptic glutamate release and Ca^{2+} entry

Release of glutamate involves membrane fusion of a 40 nm synaptic vesicle, generating a sharp diffusion neurotransmitter gradient inside and outside the cleft [23, 34]. Similarly, Ca^{2+} entering presynaptic boutons through a cluster of voltage-gated Ca^{2+} channels dissipates orders of magnitude at nanoscopic distances from the channel mouth [15, 16, 22]. Thus, when the respective fluorescent indicators are present they should in both cases generate a nanoscopic signal hotspot. In recorded images such hotspots will be blurred by the microscope's PSF and the inherent experimental noise. However, the noise could be reduced by repeated imaging whereas the PSF maximum (or centroid) coordinate normally provides 'stochastic localisation' of the signal point source. Taking advantage of these simple principles, we were able to show that the present method could, in theory, provide localisation of the preferred regions of glutamate release and Ca^{2+} entry sites, beyond the diffraction limit.

In the case of small axonal boutons, this procedure has to account for two important uncertainties. Firstly, the extent of the microscope's PSF in the z direction (0.8-1.2 µm) is compatible with the bouton size, which is further exacerbated by any focus fluctuations. In the *x*-

y plane, however, laser scanning 'resolution' is below the diffraction limit thus providing roughly uniform excitation across the bouton. This suggests that the recorded *x*-*y* image of the bouton will effectively represent its projection onto the focal plane, overestimating any membrane-bound fluorometric signal (such as that of iGluSnFR) near the visible bouton edges. We suggest that such overestimation could be corrected using trigonometric relationships for planar projection of a sphere. This correction is not required for the FLIM readout of [Ca^{2+}] because this time-domain measure is independent of the volume or concentration of the indicator. Still, the FLIM signal registered in the *x*-*y* plane will have been averaged along the PSF *z*-axis and thus might dilute the magnitude of local [Ca^{2+}] hotspots.

Secondly, and consequently, sub-diffraction localisation in the current settings is feasible only in the *x*-*y* plane whereas in the *z* plane the signal location is more uncertain. In future method adaptations, however, this uncertainty could be greatly reduced by obtaining a *z*-stack of images over the region of interest, in which the respective maxima in the *z* direction could be readily recovered [35].

METHODS

Organotypic slice culture preparation

Organotypic hippocampal slice cultures were prepared and grown with modifications to the interface culture method [36] from P6–8 Sprague-Dawley rats, in accordance with the European Commission Directive (86/609/EEC) and the United Kingdom Home Office (Scientific Procedures) Act (1986). 300 µm thick, isolated hippocampal brain slices were sectioned using a Leica VT1200S vibratome in ice-cold sterile slicing solution consisting (in mM) of Sucrose 105, NaCl 50, KCl 2.5, NaH2PO4 1.25, MgCl2 7, CaCl2 0.5, Ascorbic acid 1.3, Sodium pyruvate 3, NaHCO3 26 and Glucose 10. Following washes in culture media consisting of 50% Minimal Essential Media, 25% Horse Serum, 25% Hanks Balanced Salt solution, 0.5% L-Glutamine, 28 mM Glucose and the antibiotics penicillin (100U/ml) and streptomycin (100 µg/ml), three to four slices were transferred onto each 0.4 µm pore membrane insert (Millicell-CM, Millipore, UK), kept at 37ºC in 5% CO2 and fed by medium exchange for a maximum of 21 days in vitro (DIV).

Biolistic transfection of iGluSnFR variants

Second generation iGluSnFR variants SF-iGluSnFR.A184S and SF-iGluSnFR.A184V [7] were expressed under a synapsin promoter in CA3 pyramidal cells in organotypic slice cultures using biolistic transfection techniques adapted from manufacturer's instructions. In brief, 6.25 mg of 1.6 micron Gold micro-carriers were coated with 30µg of SF-iGluSnFR plasmid. Organotypic slice cultures at 5DIV were treated with culture media containing 5 µM Ara-C overnight to reduce glial reaction following transfection. The next day cultures were shot using the Helios gene-gun system (Bio-Rad) at 120psi. The slices were then returned to standard culture media the next day and remained for 5-10 days before experiments were carried out.

Axon tracing and imaging in single or multiple pre-synaptic boutons

We used a Femtonics Femto2D-FLIM imaging system, integrated with patch-clamp electrophysiology (Femtonics, Budapest) and linked on the same light path to two femtosecond pulse lasers MaiTai (SpectraPhysics-Newport) with independent shutter and intensity control.

Patch pipettes were prepared with thin walled borosilicate glass capillaries (GC150-TF, Harvard apparatus) with open tip resistances 2.5-3.5 MΩ. For CA3 pyamidal cells internal solution contained (in mM) 135 potassium methanesulfonate, 10 HEPES, 10 di-Tris-Phosphocreatine, 4 MgCl2, 4 Na2-ATP, 0.4 Na-GTP (pH adjusted to 7.2 using KOH, osmolarity 290–295), and supplemented with Cal-590 (300 µM; AAT Bioquest) for FLIM imaging.

Pre-synaptic imaging was carried out using an adaptation of pre-synaptic glutamate and Ca^{2+} imaging methods previously described [8]. Cells were first identified as iGluSnFR expressing using two-photon imaging at 910 nm and patched in whole cell mode as above. Following break-in, 30-45 minutes were allowed for Cal-590 to equilibrate across the axonal arbour. Axons, identified by their smooth morphology and often tortuous trajectory, were followed in frame scan mode to their targets and discrete boutons were identified by criteria previously demonstrated to reliably match synaptophysin labelled punctae [37].

For fast imaging of action-potential mediated iGluSnFR and Cal-590 fluorescence transients at single boutons a spiral shaped ("tornado") scan line was placed over the bouton of interest (described further in the text), which was then scanned at a sampling frequency of ~500 Hz with excitation at 910 nm. For multi-bouton imaging point-scans were made with a temporal resolution ~250 Hz; usage described further in text and figure legend. Following a baseline period action potentials initiated by brief positive voltage steps in voltage clamp mode (V_m holding -70mV) were given with an interval of 50 ms.

Cal-590 FLIM readout of Ca^{2+} concentration in small axonal boutons

Using the scanning methodologies described above the line-scan data were recorded by both standard analogue integration in Femtonics MES and in TCSPC in Becker and Hickl SPCM using dual HPM-100 hybrid detectors. FLIM line scan data were collected as previously described [12, 13] and stored as 5D-tensors (*t*,*x*,*y*,*z*,*T*) and analysed with custom written data analysis software available at (https://github.com/zhengkaiyu/FIMAS). Since morphological data was not of value when scanning only within the bouton, where present *x*, *y* and *z* data were summed along their respective axes. To accurately determine presynaptic [Ca^{2+}] dynamics during the burst of action potentials induced in FLIM mode, the recorded photon counts were summed across all trials to produce numbers high enough for the Normalized Total Counts (NTC) measure.

REFERENCES

1. Emptage, N.J., Reid, C.A. & Fine, A. Calcium stores in hippocampal synaptic boutons mediate short-term plasticity, store-operated Ca2+ entry, and spontaneous transmitter release. *Neuron* **29**, 197-208 (2001).
2. Branco, T., Staras, K., Darcy, K.J. & Goda, Y. Local dendritic activity sets release probability at hippocampal synapses. *Neuron* **59**, 475-485 (2008).
3. Oertner, T.G., Sabatini, B.L., Nimchinsky, E.A. & Svoboda, K. Facilitation at single synapses probed with optical quantal analysis. *Nature Neurosci.* **5**, 657-664 (2002).
4. Emptage, N.J., Reid, C.A., Fine, A. & Bliss, T.V. Optical quantal analysis reveals a presynaptic component of LTP at hippocampal Schaffer-associational synapses. *Neuron* **38**, 797-804 (2003).
5. Dittman, J. & Ryan, T.A. Molecular Circuitry of Endocytosis at Nerve Terminals. in *Annual Review of Cell and Developmental Biology* 133-160 (2009).

6. Marvin, J.S., *et al.* An optimized fluorescent probe for visualizing glutamate neurotransmission. *Nature Methods* **10**, 162-170 (2013).
7. Marvin, J.S., *et al.* Stability, affinity and chromatic variants of the glutamate sensor iGluSnFR. *BioRxiv*, /doi.org/10.1101/235176 (2018).
8. Jensen, T.P., Zheng, K., Tyurikova, O., Reynolds, J.P. & Rusakov, D.A. Monitoring single-synapse glutamate release and presynaptic calcium concentration in organised brain tissue. *Cell Calcium* **64**, 102-108 (2017).
9. Schneggenburger, R. & Neher, E. Intracellular calcium dependence of transmitter release rates at a fast central synapse. *Nature* **406**, 889-893 (2000).
10. Neher, E. & Sakaba, T. Multiple roles of calcium ions in the regulation of neurotransmitter release. *Neuron* **59**, 861-872 (2008).
11. Eggermann, E., Bucurenciu, I., Goswami, S.P. & Jonas, P. Nanodomain coupling between Ca(2)(+) channels and sensors of exocytosis at fast mammalian synapses. *Nat Rev Neurosci* **13**, 7-21 (2012).
12. Zheng, K., *et al.* Time-resolved imaging reveals heterogeneous landscapes of nanomolar Ca^{2+} in neurons and astroglia. *Neuron* **88**, 277-288 (2015).
13. Zheng, K., Jensen, T.P. & Rusakov, D.A. Monitoring intracellular nanomolar calcium using fluorescence lifetime imaging. *Nature Protocols* **13**, 581-597 (2018).
14. Tischbirek, C., Birkner, A., Jia, H., Sakmann, B. & Konnerth, A. Deep two-photon brain imaging with a red-shifted fluorometric Ca2+ indicator. *Proc Natl Acad Sci U S A* **112**, 11377-11382 (2015).
15. Schneggenburger, R. & Neher, E. Presynaptic calcium and control of vesicle fusion. *Curr Opin Neurobiol* **15**, 266-274 (2005).
16. Vyleta, N.P. & Jonas, P. Loose coupling between Ca2+ channels and release sensors at a plastic hippocampal synapse. *Science* **343**, 665-670 (2014).
17. Zheng, K. & Rusakov, D.A. Efficient integration of synaptic events by NMDA receptors in three-dimensional neuropil. *Biophys J* **108**, 2457-2464 (2015).
18. Zheng, K., Scimemi, A. & Rusakov, D.A. Receptor actions of synaptically released glutamate: the role of transporters on the scale from nanometers to microns. *Biophys J* **95**, 4584-4596 (2008).
19. Scott, R. & Rusakov, D.A. Main determinants of presynaptic Ca^{2+} dynamics at individual mossy fiber-CA3 pyramidal cell synapses. *J. Neurosci.* **26**, 7071-7081 (2006).
20. Ermolyuk, Y.S., *et al.* Independent regulation of basal neurotransmitter release efficacy by variable Ca^{2+} influx and bouton size at small central synapses. *PLoS Biol* **10**, e1001396 (2012).
21. Fenton, A.A. & Muller, R.U. Place cell discharge is extremely variable during individual passes of the rat through the firing field. *Proc Natl Acad Sci U S A* **95**, 3182-3187 (1998).
22. Zucker, R.S. & Fogelson, A.L. Relationship between transmitter release and presynaptic calcium influx when calcium enters through discrete channels. *Proc Natl Acad Sci U S A* **83**, 3032-3036 (1986).
23. Savtchenko, L.P., Sylantyev, S. & Rusakov, D.A. Central synapses release a resource-efficient amount of glutamate. *Nat Neurosci* **16**, 10-12 (2013).
24. Grienberger, C. & Konnerth, A. Imaging Calcium in Neurons. *Neuron* **73**, 862-885 (2012).
25. Ross, W.N. Understanding calcium waves and sparks in central neurons. *Nature Rev. Neurosci.* **13**, 157-168 (2012).
26. Faas, G.C., Raghavachari, S., Lisman, J.E. & Mody, I. Calmodulin as a direct detector of Ca2+ signals. *Nature Neurosci.* **14**, 301-304 (2011).
27. Regehr, W.G., Delaney, K.R. & Tank, D.W. The role of presynaptic calcium in short-term enhancement at the hippocampal mossy fiber synapse. *J Neurosci* **14**, 523-537 (1994).
28. Scott, R., Ruiz, A., Henneberger, C., Kullmann, D.M. & Rusakov, D.A. Analog modulation of mossy fiber transmission is uncoupled from changes in presynaptic Ca2+. *J. Neurosci.* **28**, 7765-7773 (2008).

29. Paredes, R.M., Etzler, J.C., Watts, L.T., Zheng, W. & Lechleiter, J.D. Chemical calcium indicators. *Methods* **46**, 143-151 (2008).
30. Grienberger, C. & Konnerth, A. Imaging calcium in neurons. *Neuron* **73**, 862-885 (2012).
31. Helmchen, F. & Denk, W. Deep tissue two-photon microscopy. *Nat Methods* **2**, 932-940 (2005).
32. Forsythe, I.D. Direct patch recording from identified presynaptic terminals mediating glutamatergic EPSCs in the rat CNS in vitro. *J. Physiol.* **479**, 381-387 (1994).
33. Wu, J., *et al.* Genetically Encoded Glutamate Indicators with Altered Color and Topology. *ACS Chem Biol* (2018).
34. Sylantyev, S., *et al.* Electric fields due to synaptic currents sharpen excitatory transmission. *Science* **319**, 1845-1849 (2008).
35. Hajj, B., El Beheiry, M., Izeddin, I., Darzacq, X. & Dahan, M. Accessing the third dimension in localization-based super-resolution microscopy. *Phys Chem Chem Phys* **16**, 16340-16348 (2014).
36. Stoppini, L., Buchs, P.A. & Muller, D. A simple method for organotypic cultures of nervous tissue. *J. Neurosci. Meth.* **37**, 173-182 (1991).
37. Rusakov, D.A. & Fine, A. Extracellular Ca^{2+} depletion contributes to fast activity-dependent modulation of synaptic transmission in the brain. *Neuron* **37**, 287-297 (2003).
38. Sylantyev, S., Jensen, T.P., Ross, R.A. & Rusakov, D.A. Cannabinoid- and lysophosphatidylinositol-sensitive receptor GPR55 boosts neurotransmitter release at central synapses. *Proc Natl Acad Sci U S A* **110**, 5193-5198 (2013).

ACKNOWLEDGEMENTS

This work was supported by the Wellcome Trust Principal Fellowship, European Research Council Advanced Grant, Medical research Council, Biology and Biotechnology Research Council (all UK), EXTRABRAIN Marie Curie Action (European Commission). The authors thank Mayeul Collot, University of Strasbourg, for generous donation of the Calcium Ruby-nano.

AUTHORS CONTRIBUTIONS

T.P.J. designed and carried out imaging experiments; K.Z. designed and implemented time-resolved imaging methods; N.C. carried out slice preparations, transfection and molecular biology protocols; J.S.M. and L.L.L. developed and provided SF-iGluSnFR glutamate sensor variants; T.P.J., K. Z. and D.A.R. analysed the data; D.A.R. narrated the study and wrote the draft; all authors contributed to manuscript writing.

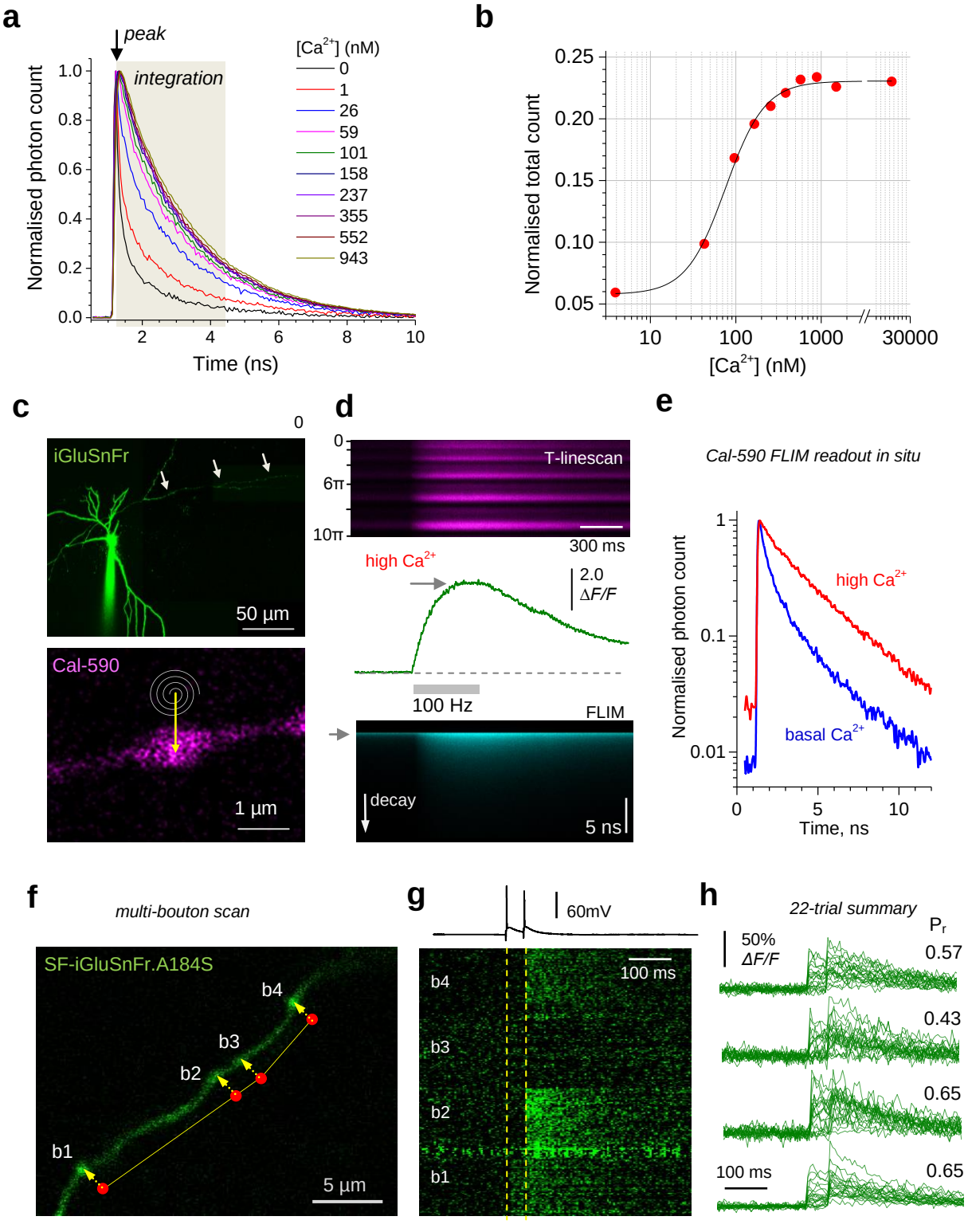

Figure 1. Fluorescence lifetime of Cal-590 provides readout of low intracellular Ca^{2+} while iGluSnFR.A184S enables multi-synapse glutamate release imaging

(a) Fluorescent lifetime decay curves of Cal-590 in a series of calibrated [Ca^{2+}]-clamped solutions finely adjusted to include appropriate intracellular ingredients [12, 13]: FLIM traces are normalised to their peak values

(at ~1.3 ns post-pulse) and the area under the decay curve over the time interval of 3 ns (tan shade) was measured to establish Normalised Total Count readout; λ_x^{2p} = 910 nm; temperature 33°C.

(b) The Cal-590 FLIM [Ca^{2+}] sensitivity estimator, normalised total count, fitted with sigmoid type function ($\chi^2 = 2.11 \cdot 10^{-5}$, $R^2 = 0.996$).

(c) *Top:* Example of a CA3 pyramidal cell (iGluSnFR channel); arrowheads, proximal part of the traced axon; patch pipette is seen. *Bottom:* Example of an axonal bouton (Cal-590 channel) traced from the cell soma; spiral line and arrow, tornado linescan applied in the middle of the bouton.

(d) Example of a single-bouton Cal-590 signal during a 500 ms 100 Hz burst of spike-inducing somatic 1 ms current pulses: recorded as a tornado linescan (*top*; ordinate, spiral rotation angle 0-10π reflects five concentric spiral circles, 2π radian/ 360º each), fluorescence intensity (integrated over the 10π spiral scan) time course (*middle*) and fluorescence decay (FLIM, *bottom*; ordinate, decay time; grey arrowhead, laser pulse onset).

(e) Intra-bouton Cal-590 fluorescence decay time course (normalised to peak) representing basal [Ca^{2+}] (blue) and peak [Ca^{2+}] (red), in the experiment shown in **d**.

(f) CA3 pyramidal cell axon fragment showing four presynaptic boutons (b1-b4), with the scanning dwell points in the bouton centres (red dots, dwell time 1.5 ms) and laser scan trajectory (dotted yellow line) illustrated.

(g) Linescan image of iGluSnFR signals recorded simultaneously (one sweep) at four boutons shown in **f** as indicated, during somatic generation of two action potentials 50 ms apart (top trace, current clamp); glutamate releases and failures can be seen.

(h) A summary of 22 trials in the experiment shown in **f**-**g** (traces show single-trial iGluSnFR intensity readout at the four bouton centres); Pr, average probability of the first release event; traces indicate paired-pulse facilitation.

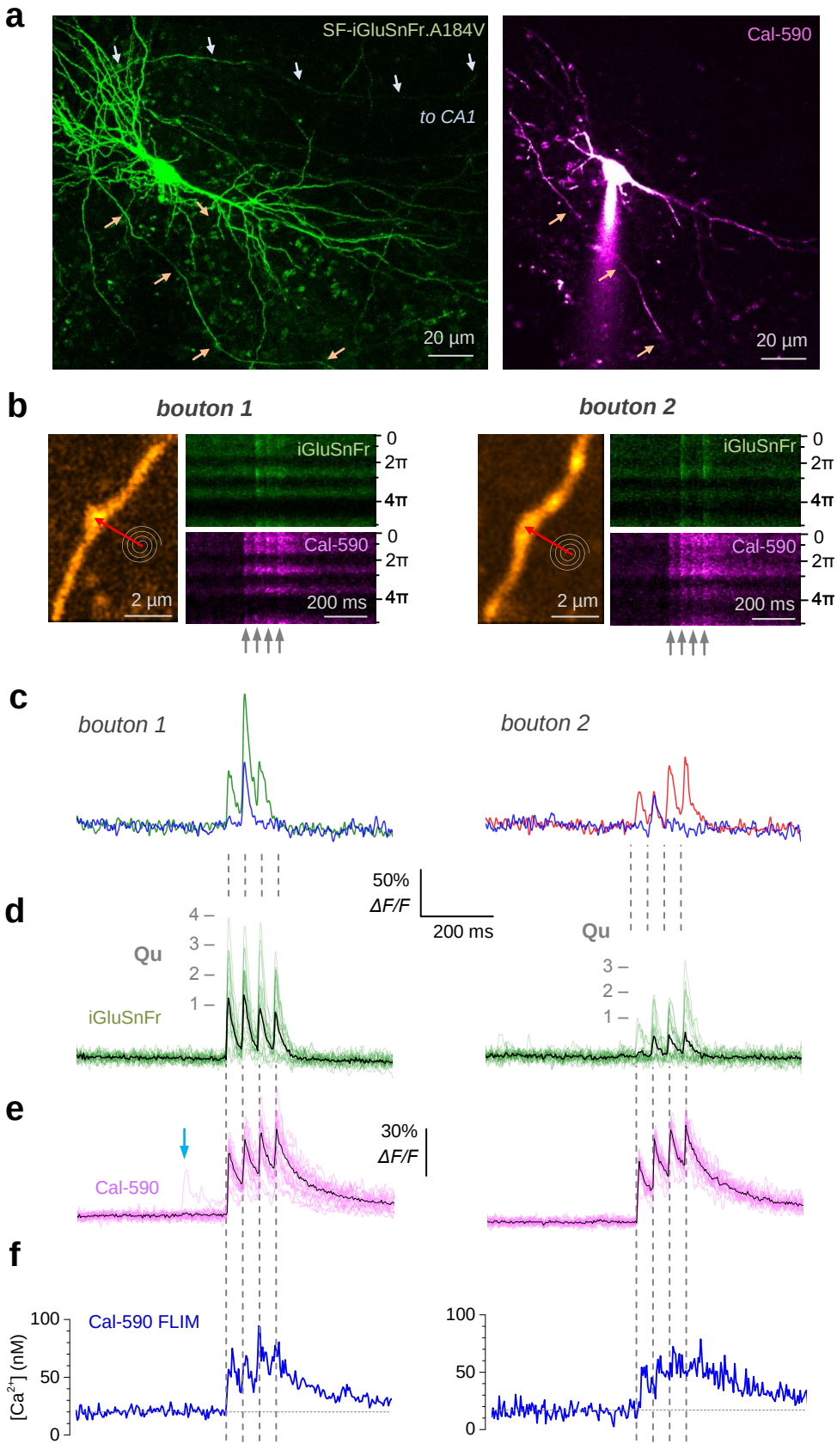

Figure 2. Multiplex imaging of quantal glutamate release and presynaptic Ca^{2+} dynamics.

(a) CA3 pyramidal cell, organotypic slice. *Left*: green emission channel, biolistic transfection with SF-iGluSnFR.A184V [7] (6.25 mg of 1.6 µm Gold microcarriers coated with 30 µg plasmid; Bio-Rad Helios gene-gun at 120psi); arrows (white/orange), two main axonal branches. Planar projection, ~60 µm deep image *z*-stack, λ_x^{2p} =910 nm. *Right*, red emission channel (fragment, ~20 µm *z*-stack projection), after whole-cell patch and dialysis with Cal-590 (300 µM); patch pipette is seen.

(b) Imaging presynaptic function at two axonal boutons (traced into CA1 from one CA3 pyramidal cell, as detailed earlier [8, 38]): *left panels*, morphological image (green channel); spiral and red arrow, tornado scan positions; *right panels*, examples of tornado line-scans (spiral rotation angle 0-5π reflects 2.5 concentric spiral circles, 2π radian/360° each) during four somatically evoked action potentials (20 Hz, grey arrows); shown in iGluSnFR (green) and Cal-590 (magenta) channels, as indicated; note glutamate release failures in the iGluSnFR channel.

(c) Two characteristic single-trial, one-sweep recordings (red and blue lines, iGluSnFR channel) depicting individual quantal releases and failures, in the two boutons, as indicated.

(d) Summary of glutamate release kinetics (iGluSnFR channel) documented in 20 sequential trials 1 min apart (green, individual trials; black, average trace) in boutons 1 and 2, as indicated; **Qu** (1-4), approximate scale for individual released glutamate quanta; note presynaptic short-term depression and facilitation in boutons 1 and 2, respectively, supplied by the same axon.

(e) Cal-590 fluorescence intensity signal $\Delta F/F$ (red channel) recorded simultaneously in the same test (magenta, individual trials; black, average trace); blue arrow, a spontaneous Ca^{2+} entry event, which is not accompanied by glutamate release (see **d**).

(f) Dynamics of free presynaptic [Ca^{2+}] averaged over 20 trials: signal readout with Cal-590 FLIM (normalised photon count), converted to [Ca^{2+}]. Note that these data reflect free ion concentration volume-equilibrated and time-averaged over 5-10 ms.

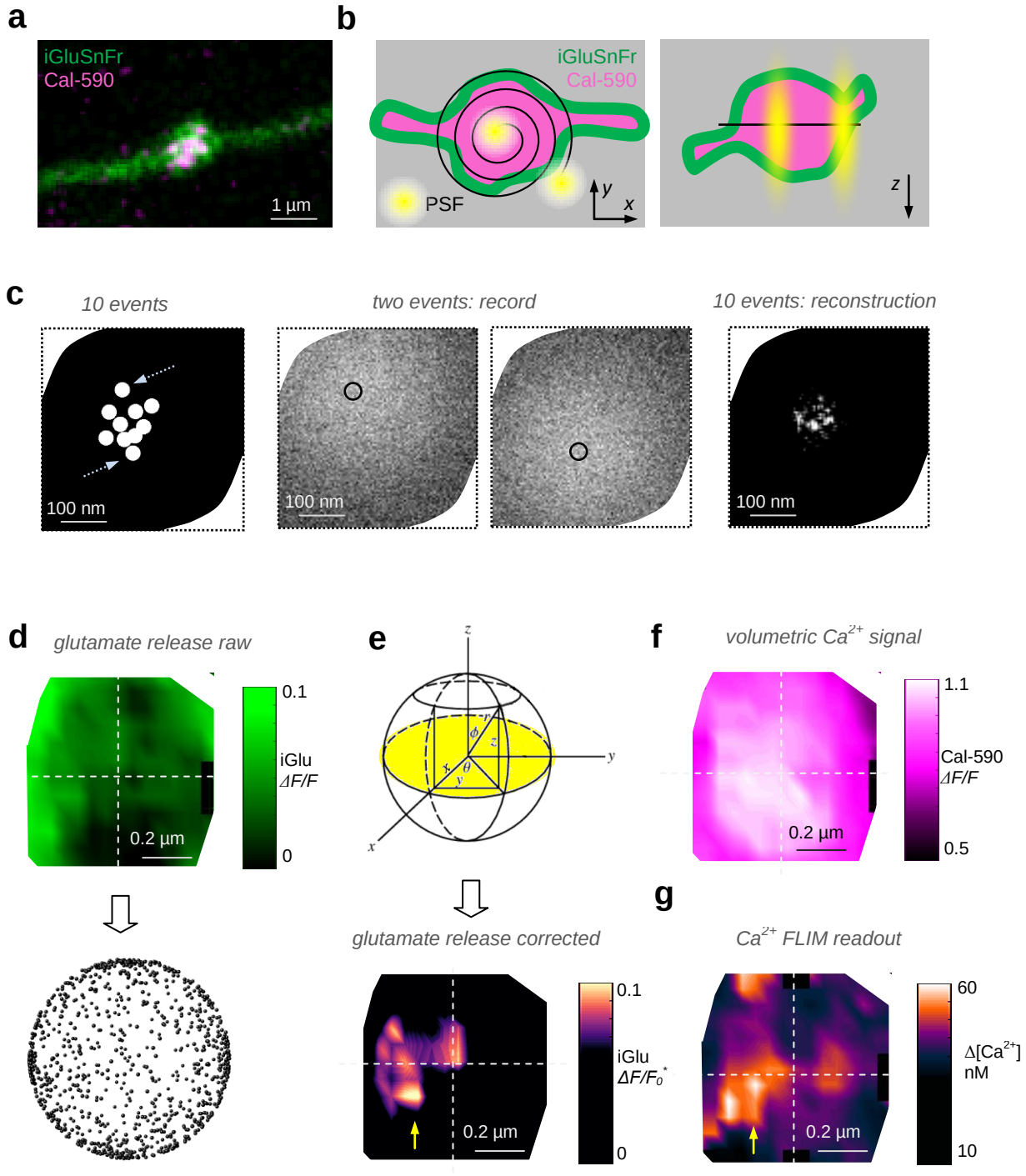

Figure 3. Multi-exposure, multiplex imaging enabling stochastically reconstructed localisation of Ca^{2+} entry and glutamate release in individual axonal boutons.

(a) An example of a CA3-CA1 axonal bouton, a merged-two-channel image (SF-iGluSnFR.A184V green, Cal-590 magenta).

(b) Axonal bouton diagram illustrating imaging (laser scanning) settings, in the *x*-*y* (left) and *z* (right) plane, with membrane-bound expression of iGluSnFR (green) and cytosolic Cal-590 (magenta); black spiral (left) and straight line (right), approximate tornado linescan trajectory; yellow spots illustrate typical point-spread function (PSF): note that the *x*-*y* plane image represents, in large part, *z*-projection of the bouton.

(c) Sub-diffraction localisation through multi-exposure noise reduction: illustration of first principles. *Left*: diagram depicting the loci of ten consecutive fluorescent events to be imaged; *middle*, characteristic images of two events (circles, arrows on the left), with the PSF (~200 nm wide) and typical noise (~30% of the signal amplitude) added; *right*, the brightest part (>90% of peak) in the 10-event average record, revealing the expected (likely) localisations of the events, with sub-diffraction resolution.

(d) *Top***,** ROI of an axonal bouton showing the average (20 trials) heat map of the iGluSnFR intensity signal (experiments as Fig. 2); *bottom*, schematic showing that the projection of sphere-like objects (such as axonal boutons) with uniform surface distribution of the sources of fluorescence (dots) reports highly overestimated signal density towards the projection edges.

(e) *Top*, geometry of the sphere projection onto a microscope view *x*-*y* plane (yellow), using spherical coordinates; the signal density on the sphere surface (as in **d** bottom) is projected with a factor of $1 / \cos(\varphi)$. *Bottom*, iGluSnFR intensity signal heat map $F(r_{xy},\theta)$, with raw data (shown in **d** top, cylindrical coordinates, origin at the centre) corrected for the sphere-like projection: $F(r_{xy},\theta) = F_0(r_{xy},\theta)(1-r^2/r_{xy}^2)^{1/2}$ where $F_0(r_{xy},\theta)$ is the recorded brightness, r_{xy} is the distance between the centre and the point of interest, and r is the distance between the centre and the visible edge of the axonal bouton (see Supplementary Fig. 3 for technical details and basic assumptions involved).

(f) The average intensity signal of cytosolic Cal-590, with the signal amplitude correlated with the imaged indicator volume.

(g) The average (20 trials) heat map of the Cal-590 FLIM readout, which is volume-independent; signal is resolved within the *x*-*y* plane but integrated (and thus possibly diluted) along the *z*-axis. Arrows in **f** and **g** point to the likely site of nano-colocalisation.

SUPPLEMENTARY FIGURES

a

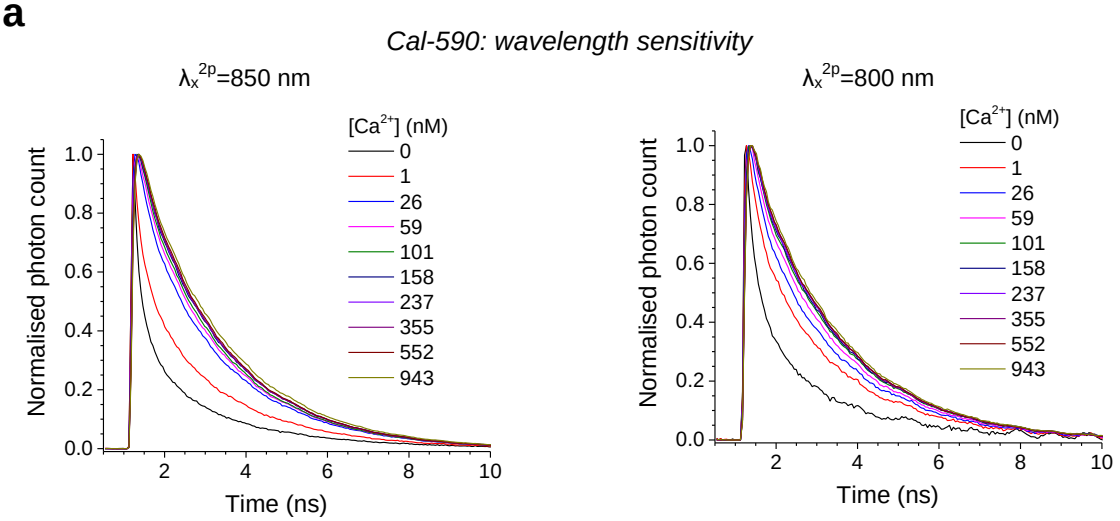

b

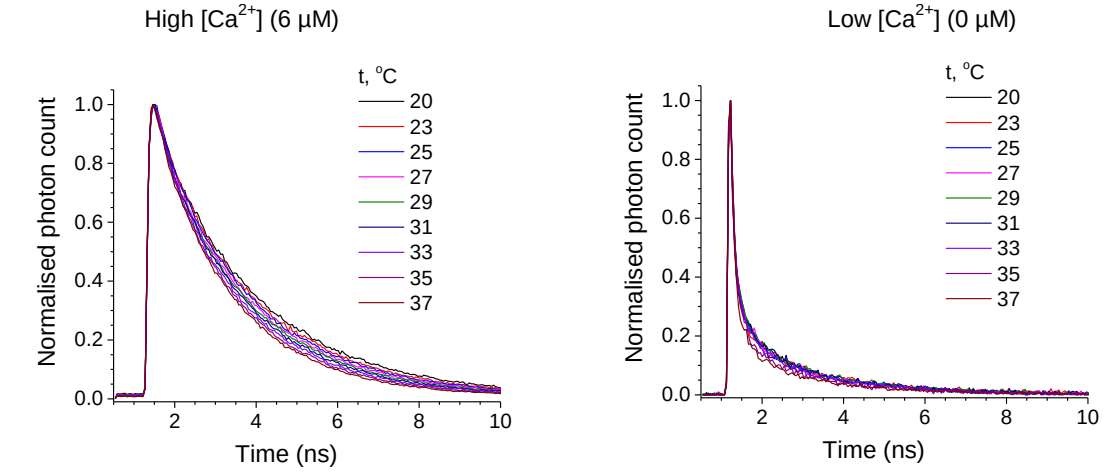

c

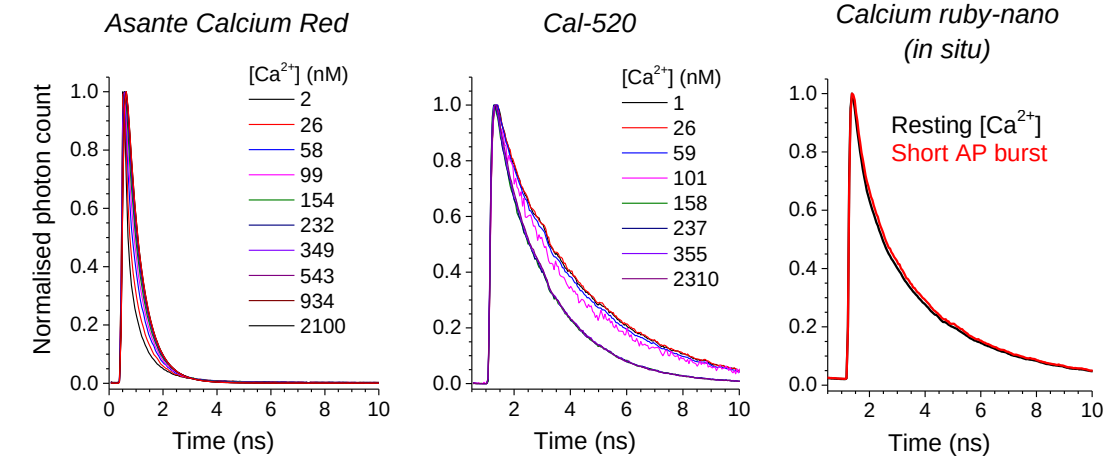

Supplementary Figure 1. Cal-590 fluorescence lifetime sensitivity to excitation wavelength and temperature / viscosity.

(a) Cal-590 lifetime sensitivity to [Ca^{2+}] under different two-photon excitation wavelength, 850 nm and 800 nm, as indicated (temperature 33ºC). The detected sensitivity range for 0-200 nM [Ca^{2+}] is narrower than that for the optimal excitation wavelength of 910 nm (Fig. 1a-b).

(b) Fluorescence decay of Cal-590 under saturating (left) and zero-clamped (right) [Ca^{2+}], over the range of experimentally relevant temperatures, as indicated (viscosity).

(c) Testing the fluorescence decay [Ca^{2+}] sensitivity for Asante Calcium Red, Cal-520, and ruby-nano, as indicated: the first two were evaluated using the standard FLIM calibration procedure as in **a-b** whereas Calcium ruby-nano was tested *in situ* (axonal bouton, CA3 pyramidal cell, organotypic hippocampal slices), by comparing its fluorescence decay in resting conditions (black) and during peak intensity response to a burst of four action potentials (at 20 Hz, red), as indicated; recordings at λ_x^{2p} = 910 nm, 33ºC.

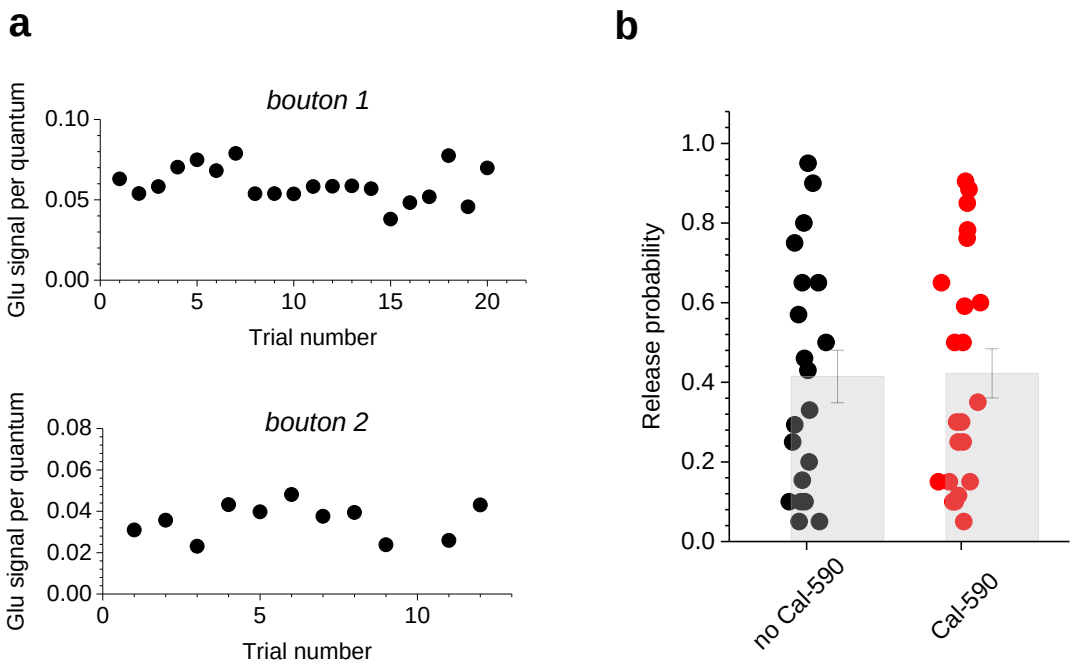

Supplementary Figure 2. Quantal size dynamics and the effect of Cal-590 dialysis on release probability.

(a) Trial-to-trial dynamics of the iGluSnFr signal representing a single quantum of glutamate release from bouton 1 and 2 (shown in Fig. 2). *Abscissa*, trial number (in bouton 2, traces after the 12th trial showed no detectable glutamate release). *Ordinate*, average $\Delta F/F$ fluorescence signal of iGluSnFr per one release quantum; the value was calculated by measuring the time-average $\Delta F/F$ signal over the time interval corresponding to four evoked spikes (250 ms, onset at the foot of first Ca^{2+} or iGluSnFr signal) divided by the number of detected released quanta.

(b) Probability of evoked glutamate release (in response to a single action potential) in axonal boutons of CA3 pyramidal cells (organotypic hippocampal slices) expressing iGluSnFr, with and without Cal-590 (300 µM) being loaded and equilibrated in whole-cell mode, as indicated. Dots, individual bouton recordings; bar graph, mean ± s.e.m. (0.41 ± 0.07 and 0.42 ± 0.06, n = 20 and n = 22, without and with Cal-590, respectively).

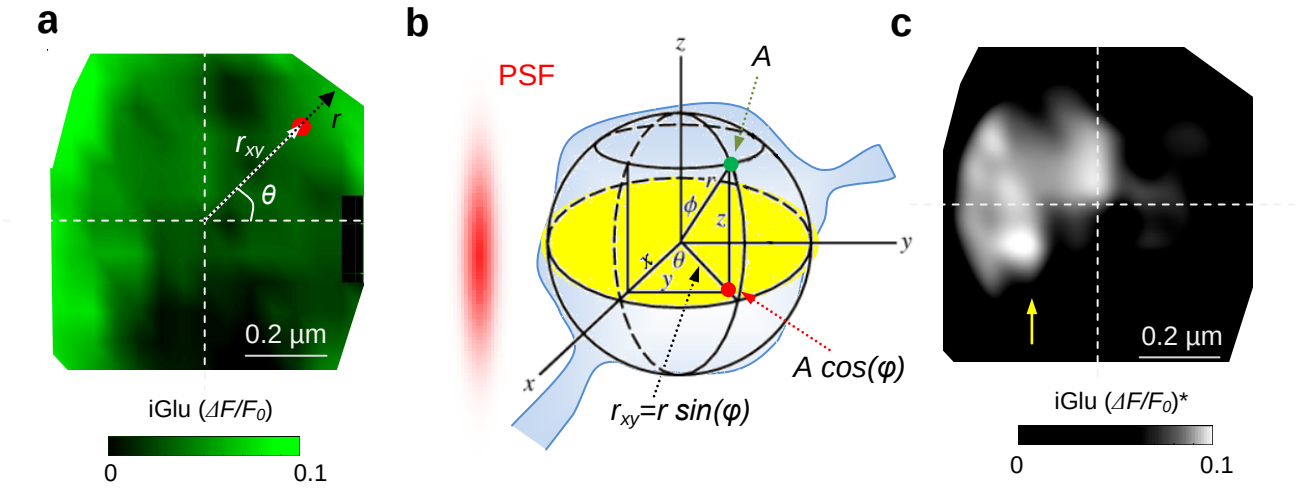

Supplementary Figure 3. Stereological correction for the signal density on spherical surface projected onto the (microscope view) plane.

(a) ROI of the axonal bouton depicting the 20-trial-average heat map of the iGluSnFr signal (as in Fig. 3d) in the microscope plane view; each trial consists of four action potential at 20 Hz, with varied number of glutamate quanta released; red dot, example point of interest shown at a distance r_{xy} from the ROI (bouton) centre, with the centre-edge distance r.

(b) Schematic of the geometric relationships representing (approximately) the microscope's point-spread function (PSF, red shade) and a sphere-like bouton (blue shape) projecting its shape onto the microscope focal plane (yellow); spherical coordinates indicated; other notations correspond to those in **a**; a small sphere surface element of area A, indicated by green dot, will project onto the red dot location (in yellow plane) as area $A \cdot cos(\varphi)$, as indicated.

This relationship relies on the assumption that during laser scanning the excitation is distributed uniformly across the bouton (because of the sub-diffraction scanning resolution in the *xy* plane and the bouton-compatible PSF size in the z direction, further exacerbated by focus fluctuation). In that case, in spherical coordinates, the differential (infinitesimal) element of the sphere surface (indicated by green dot) has an area of $r^2 \cdot sin(\varphi) d\varphi d\theta$ whereas its projection onto the z=0 plane has an area of $r^2 \cdot sin(\varphi) \cdot cos(\varphi)\ d\varphi d\theta$. The ratio between the latter and the former is $cos(\varphi)$, implying that the signal density in the planar projection is boosted by factor $1 / cos(\varphi)$. Thus applying the factor $cos(\varphi) = (1 - sin^2(\varphi))^{1/2} = (1 - r_{xy}^2 / r^2)^{1/2}$ to the image intensity should provide the projection-corrected value.

(c) Image in panel **a** corrected for surface projection, where pixel brightness at each location $F(r_{xy},\theta)$ is corrected using $F(r_{xy},\theta) = F_0(r_{xy},\theta)(1 - r^2 / r_{xy}^2)^{1/2}$ where $F_0(r_{xy},\theta)$ is the

recorded brightness (as in panel **a**), r_{xy} is the distance between the centre and the point of interest (as in panels **a-b**), and r is the distance between the centre and the visible edge of the axonal bouton (as in panels **a-b**). Arrow indicates the area of the highest signal intensity post-correction.